IOPscience iopscience.iop.org

Home Search Collections Journals About Contact us My IOPscience

Simulation study on electrical characteristic of AlGaN/GaN high electron mobility transistors with AlN spacer layer

This content has been downloaded from IOPscience. Please scroll down to see the full text.

2014 Jpn. J. Appl. Phys. 53 04EF08

(http://iopscience.iop.org/1347-4065/53/4S/04EF08)

View the table of contents for this issue, or go to the journal homepage for more

Download details:

IP Address: 140.113.38.11
This content was downloaded on 25/12/2014 at 03:14

Please note that terms and conditions apply.

Japanese Journal of Applied Physics 53, 04EF08 (2014)
http://dx.doi.org/10.7567/JJAP.53.04EF08 **REGULAR PAPER**

Simulation study on electrical characteristic of AlGaN/GaN high electron mobility transistors with AlN spacer layer

Niraj Man Shrestha[1], Yiming Li[2*], and Edward Yi Chang[1*]

[1]Compound Semiconductor Device Laboratory, Department of Material Science and Engineering, National Chiao Tung University, Hsinchu 300, Taiwan
[2]Parallel and Scientific Computing Laboratory, Department of Electrical and Computer Engineering, National Chiao Tung University, Hsinchu 300, Taiwan
E-mail: ymli@faculty.nctu.edu.tw; edc@mail.nctu.edu.tw

Received September 24, 2013; revised November 20, 2013; accepted November 25, 2013; published online February 24, 2014

Two-dimensional electron gas (2DEG) property is crucial for the performance of GaN-based high electron mobility transistors (HEMTs). The 2DEG-related concentration and mobility can be improved as device's performance booster. Electrical characteristics of AlGaN/AlN/GaN HEMT are numerically simulated and compared with conventional AlGaN/GaN HEMT. The main findings of this study indicate that 2DEG's concentration level is increased when a spacer layer of AlN in the interface of AlGaN/AlN/GaN is inserted owing to large conduction band off set, high polarization field, and high barrier. Notably, when a thin spacer layer of AlN is introduced, the 2DEG's distribution virtually shifts away from the interface which reduces the interface scattering. The scattering appearing in conventional AlGaN/GaN HEMT includes alloy and interface roughness scatterings. They are reduced in AlGaN/AlN/GaN HEMT due to binary nature of AlN material. A critical thickness of spacer layer for mobility is 0.5 nm and the maximum drain current and transconductance (G_m) are at 1.5 and 1.2 nm thickness of AlN spacer layer. Increasing thickness of AlN spacer layer deteriorates the ohmic resistance of source/drain contact and hence degrades the performance of device beyond 1.5-nm-thick AlN spacer layer. © 2014 The Japan Society of Applied Physics

1. Introduction

GaN-based high electron mobility transistors (HEMTs) have attracted a great deal of attention for high-frequency and high-power microwave applications because nitride-based material systems have desirable fundamental physical properties, such as a large band gap (3.4 eV), high breakdown field (about 3×10^6 V/cm) and strong spontaneous and piezoelectric polarization fields. A unique feature of GaN-based HEMTs is high sheet carrier concentration (1×10^{13} cm^{-2}), which is achieved in the channel not only due to large band gap discontinuity[1] at interface but also due to piezoelectric and spontaneous polarization effect without intentionally doping barrier layer.[2–4] Because of these advantageous material properties, GaN and its related alloys have been used in a variety of light-emitting devices and electron devices on a commercial basis. Nevertheless, more technological innovations are needed to realize high-efficiency, highly reliable and low-cost devices. High power density is one of key parameters for diverse power devices. In order to increase the power density, the product of electron concentration and electron mobility should be maximized.[5,6] To improve device's performance, various barrier and channel alternatives have been studied in nitride-based HEMTs.[7,8] Carrier's concentration level can be increased by increasing Al mole fraction and AlGaN barrier layer thickness.[9,10] However, when the Al content of AlGaN layer increases, surface quality of AlGaN layer is degraded and then reduces the two-dimentional electron gas (2DEG) mobility.[9,11] The existence of the different scatterings, such as acoustic and optical phonons scattering,[12,13] ionized impurity scattering, interface roughness scattering,[14] dislocation scattering, and alloy disorder scattering[15–18] play major role to limit the mobility of 2DEG in conventional AlGaN/GaN HEMT. These scatterings are unique to GaN-based HEMTs due to large dislocation density and strong polarization effects.

An additional thin AlN spacer between AlGaN and GaN may improve the 2DEG concentration[1] and the mobility at low temperatures.[18] It is found that, the carriers' mobility in AlGaN/AlN/GaN HEMTs is comparatively higher than that of the conventional device without AlN spacer layer.[18,19] A thin AlN spacer layer in AlGaN/GaN interface causes the reduction of alloy scattering which plays a dominant factor in the carriers' mobility. Another effect of AlN spacer layer insertion is the reduction in the forward Schottky gate current, which makes it possible to apply a high gate voltage in the transistor operation.[20] The drain current of AlGaN/AlN/GaN HEMTs is better than that of conventional AlGaN/GaN HEMTs.[21–23] Therefore, the AlN spacer layer is one of the fascinating ways to achieve high speed, high power switching device with low specific on resistance. Additionally, the thickness of AlN is important for the mobility.[19] When the thickness is changed, the polarization field and the conduction band offset are changed which also affects the 2DEG-related concentration and mobility. Therefore, to know the potential thickness of spacer layer for high power device and to know the real cause of reduction of mobility at higher spacer layer thickness will be interesting studies.

In this study, the effect of AlN spacer layer thickness on electrical characteristic in AlGaN/AlN/GaN HEMT is numerically studied. The most potential spacer layer thickness for power device is discussed. In addition, effect of the AlN layer thickness on interface roughness scattering will be highlighted. This paper is organized as follows. In Sect. 2, we introduce the device structure and simulation settings used for studying the effect of AlN spacer layer thickness on AlGaN/AlN/GaN HEMT. In Sect. 3, we report our result and examine the transport property as determined by the thickness of AlN spacer layer. Finally, we draw our conclusions and suggest future works in Sect. 4.

2. Simulation methodology

The epitaxial layer grown step and fabrication step is shown in Figs. 1(a)–1(f). The physical device studied in this paper is grown on sapphire substrates by using metal organic chemical vapor deposition system at different temperatures.

 © 2014 The Japan Society of Applied Physics

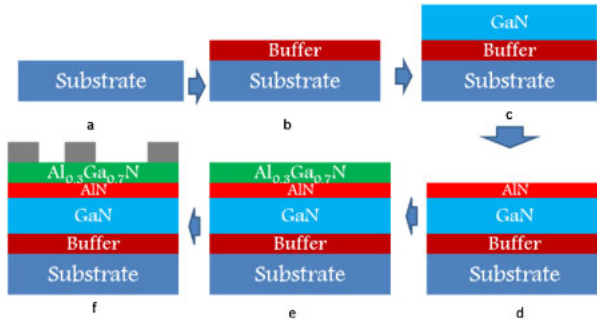

Fig. 1. (Color online) Epilayer grown and process flow of the studied AlGaN/AlN/GaN HEMT.

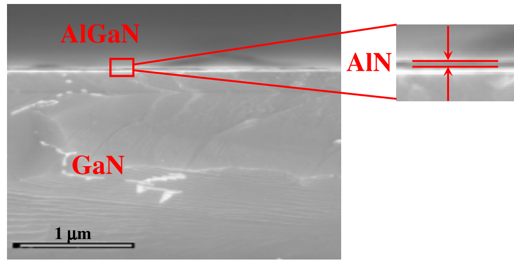

Fig. 2. (Color online) A SEM image of the AlGaN/GaN structure with the AlN spacer layer.

Entire growth process is conducted by using ammonia (NH_3), trimethylgallium (TMGa), trimethylaluminum (TMAl) as precursors and hydrogen as carrier gas. Following an AlN nucleation layer, a 2-µm-thick undoped GaN buffer is grown. A thin AlN spacer layer of varying thickness (0–2 nm) and a 25-nm-thick undoped AlGaN barrier layer are grown on top. The entire epitaxial layer is grown at high temperature. The Al mole fraction determined by using X-ray diffraction is around 30%. Figure 2 shows a scanning electron microscope (SEM) image of cross section of the fabricated AlGaN/AlN/GaN HEMT structure.

The simulated device structures of AlGaN/GaN HEMT with and without the AlN spacer layer are shown in Figs. 3(a) and 3(b), where the parameters of simulated devices are tabulated in Table I. Figure 3(a) is the device is the conventional structure without the spacer layer and Fig. 3(b) with the AlN spacer layer and both structures use the same device parameters except the thickness of AlN spacer layer. As shown in Fig. 3(b), the thickness of AlN spacer layer varies from 0 to 2 nm while keeping the total thickness of AlN and AlGaN layers at 25 nm. Notably, an insertion of thin AlN layer between AlGaN and GaN can enhance the confinement of 2DEG. Therefore, improvement of electron transport characteristic could be estimated. The spacer layer affects the transport carrier which is related to 2DEG's concentration and mobility. The band gaps of the relevant binary compounds are computed, by Eqs. (1) and (2), as a function of temperature T:

$$E_g(\mathrm{GaN}) = 3.507 - \frac{0.909 \times 10^{-3} T^2}{T + 830}, \quad (1)$$

$$E_g(\mathrm{AlN}) = 6.23 - \frac{1.799 \times 10^{-3} T^2}{T + 1462}. \quad (2)$$

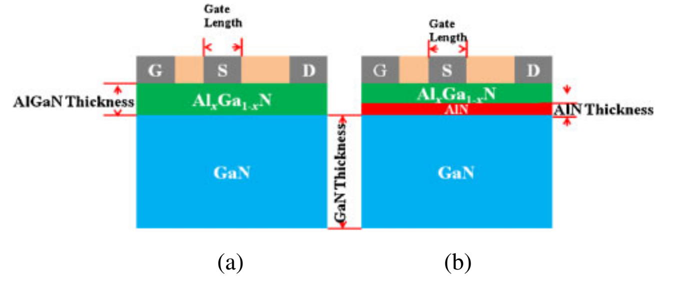

Fig. 3. (Color online) Schematic plots of the AlGaN/GaN HEMT. (a) Conventional device is without the AlN spacer layer and (b) the explored device which is with the AlN spacer layer.

Table I. Parameters used for the simulated devices.

Gate width (µm)	15
AlGaN layer thickness (nm)	25
GaN layer thickness (µm)	2
Al composition in AlGaN (%)	30
Gate length (µm)	1
AlN thickness (nm)	0, 0.3, 0.5, 1, 1.2, 1.5, 2

The band gap of ternary compound depends on composition fraction x is given by

$$E_g(\mathrm{Al}_x\mathrm{Ga}_{1-x}\mathrm{N}) = E_g(\mathrm{AlN}) + E_g(\mathrm{GaN})(1-x) - 1.3x(1-x). \quad (3)$$

Polarization is one of key mechanisms in controlling the formation of the 2DEG at the AlGaN/GaN interface. P_{PZ} of Eq. (4) is piezoelectric polarization which is related to strain tensor:

$$P_{PZ} = 2\frac{a_s - a_0}{a_0}\left(E_{31} - \frac{C_{13}}{C_{33}}E_{33}\right), \quad (4)$$

where E_{31} and E_{33} are piezoelectric constants, and C_{13} and C_{33} are elastic constants. When an $Al_xGa_{1-x}N$ grown on GaN, the piezoelectric polarization is expressed as

$$P_{PZ}(x) = (-3.2x - 1/9x^2)10^{-6}\,\mathrm{cm}^{-2}. \quad (5)$$

In addition to strain induced polarization, cations and anions are spontaneously displaced with respect to each other, producing spontaneous polarization. Then total polarization is given by

$$P_{tot} = P_{PZ} + P_{SP}. \quad (6)$$

The Schottky barrier height estimated is 1.4 V. A 2D quantum mechanically corrected device simulation is performed, where the quantum mechanical correction is considered with a density-gradient approach. Performance of device mainly depends on the carriers' mobility which is affected by various types of scattering mechanism; such as, the phonon scattering (at room temperature), the alloy disorder scattering (potential disorder from ternary alloy, at low and room temperatures), the surface roughness scattering (at low temperature), the ionized impurities scattering, the dislocation scattering, and the dipole scattering. Among these scattering mechanisms, the alloy disorder scattering is the limiting factor[14] at low and room temperatures when the carrier's concentration is high. Binary nature of AlN makes comparatively low alloy disorder scattering. Notably, the

 © 2014 The Japan Society of Applied Physics

increase in the quantum well depth and barrier directly provide even better confinement of electron concentration, and hence reduce other scatterings. Therefore, in our device simulation, the electron mobility model considers two parts; one is the low field mobility model and the other is the nitride specific high field dependent mobility model. The first low field mobility model consists of the interface roughness scattering and alloy scattering. The expression for the interface roughness scattering is given by[24]

$$\frac{1}{\mu_0^{\mathrm{I}}(N_{\mathrm{D}},T)} = a(N_{\mathrm{D}}/10^{17})\ln(1+\beta_{\mathrm{cw}}^2)/(T/300)^{1.5} + b(T/300)^{1.5} + c/\exp(\Theta/T-1), \quad (7)$$

where $\Theta = \hbar\omega_{\mathrm{LO}}/k_{\mathrm{B}}$ is related to the phonon scattering resulting from the scattering of interface roughness, $\beta_{\mathrm{cw}}^2 = 3(T/300)^2(N_{\mathrm{D}}/10^{17})^{-2/3}$, N_{D} (cm^{-3}) is ionized donor concentration, T (K) is absolute temperature. Notably, the interface roughness scattering is one of the most important factors to determine the longitudinal optical phonons; in particular, for binary compound quantum wells where the contribution from the alloy scattering is absent.[25,26] The expression for the alloy scattering, is given by[27]

$$\mu_0^{\mathrm{A}}(N_{\mathrm{D}},T) = \mu_{\min}\times(T/300)^{\beta_1} + \frac{(\mu_{\max}-\mu_{\min})\times(T/300)^{\beta_2}}{1+[N_{\mathrm{D}}/10^{17}\times(300/T)^{\beta_3}]^{\gamma(T/300)^{\beta_4}}}, \quad (8)$$

Table II. The adopted parameters in Eqs. (7) and (8).[24,27]

Θ	1065
a ($\mathrm{V\,s^{-1}\,cm^{-2}}$)	2.61×10^{-4}
b ($\mathrm{V\,s^{-1}\,cm^{-2}}$)	2.9×10^{-4}
c ($\mathrm{V\,s^{-1}\,cm^{-2}}$)	1.7×10^{-2}
V^{sat} (cm/s)	1.9064×10^{7}
α	6.12
n_1	7.2
n_2	0.786
E_0 (kV/cm)	220.89

Table III. The adopted parameters in Eq. (8).[27]

	β_1	β_2	β_3	β_4	γ
GaN	−1.02	−3.84	3.02	0.81	0.66
AlGaN	−1.33	−1.75	6.02	1.44	0.29
AlN	−1.82	−3.43	3.78	0.86	1.16

where $\mu_{\min}$ and $\mu_{\max}$ are the minimum and maximum mobility for the materials.

Therefore, the nitride specific high field dependent mobility model is[27]

$$\mu(E) = \frac{\mu_0^{\mathrm{A}}(N_{\mathrm{D}},T)\mu_0^{\mathrm{I}}(N_{\mathrm{D}},T)/[\mu_0^{\mathrm{A}}(N_{\mathrm{D}},T)+\mu_0^{\mathrm{I}}(N_{\mathrm{D}},T)] + v^{\mathrm{sat}}(E^{n_1-1}/E_0^{n_1})}{1+\alpha(E/E_0)^{n_2}+(E/E_0)^{n_1}}, \quad (9)$$

where $\mu_0^{\mathrm{I}}(N_{\mathrm{D}},T)$ and $\mu_0^{\mathrm{A}}(N_{\mathrm{D}},T)$ are calculated from Eqs. (7) and (8), v^{sat} is the saturation velocity, E is electric field, and the other parameters used in Eqs. (7)–(9) are tabulated in Tables II and III. The current characteristics of device can be evaluated through Schrödinger equation into a self-consistent computation with the Poisson equation.[28–31]

3. Results and discussion

Simulation study of electron transport and DC characteristic of the purposed AlGaN/AlN/GaN HEMT is performed in this section. We compare the results with that of conventional AlGaN/GaN HEMT to show the advantage of the spacer layer of AlN in the interface of the AlGaN/AlN/GaN of the explored device. In Sect. 3.1, we show and discuss the physical characteristic of the device. In Sect. 3.2, we report the electrical characteristics including the transport current and the transconductance.

3.1 Physical characteristic

Figure 4 illustrates the patterns of conduction band profile of the proposed AlGaN/AlN/GaN HEMT and the conventional AlGaN/GaN device. A thin AlN spacer layer in the hetero-interface of AlGaN/GaN produces large effective conduction band offset because of the potential drops across the spacer layer due to large piezoelectric and spontaneous polarization field.[32] The increase in the conduction band offset when using the thin AlN spacer layer inside the structure of AlGaN/GaN is explained by

$$\Delta E_{\mathrm{c}}^{\mathrm{AlN}} - \Delta E_{\mathrm{c}}^{\mathrm{AlGaN}} = \exp\left(\frac{\sigma_{\mathrm{AlN}}-N_{\mathrm{2D}}}{\varepsilon_{\mathrm{AlN}}}\right)d_{\mathrm{AlN}}, \quad (10)$$

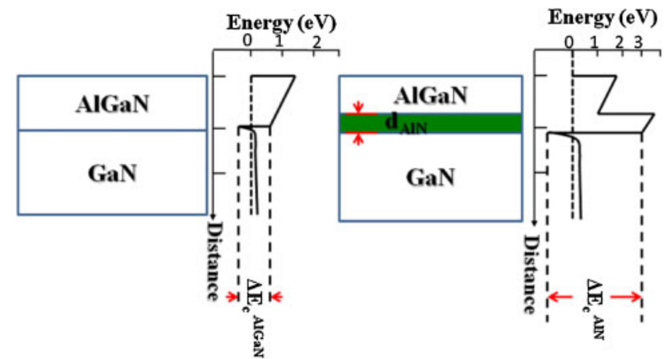

Fig. 4. (Color online) Illustration of the pattern of band diagram for the (a) AlGaN/GaN and (b) AlGaN/AlN/GaN HEMTs.

where $\Delta E_{\mathrm{c}}^{\mathrm{AlN}}$ and $\Delta E_{\mathrm{c}}^{\mathrm{AlGaN}}$ are the effective conduction band offsets between the AlGaN/AlN/GaN and the AlGaN/GaN, respectively; N_{2D} is the sheet carrier concentration of the AlGaN/AlN/GaN structure, $\varepsilon_{\mathrm{AlN}}$ is dielectric constant, σ_{AlN} is the polarization induced charge at the AlN/GaN inferface, and d_{AlN} is the thickness of AlGaN.[10] Effect of the thickness of AlN spacer layer on the conduction band offset was analyzed by means of device simulation and results are plotted as shown in Fig. 5(a). The conduction band offset becomes large when the thickness of AlN spacer layer increases. Numerically calculated values of the quantum well depth with respect to the thickness of AlN spacer layer is tabulated in Table IV. Figure 5(b) shows the quantum well depth for the device with respect to different thickness of AlN

© 2014 The Japan Society of Applied Physics

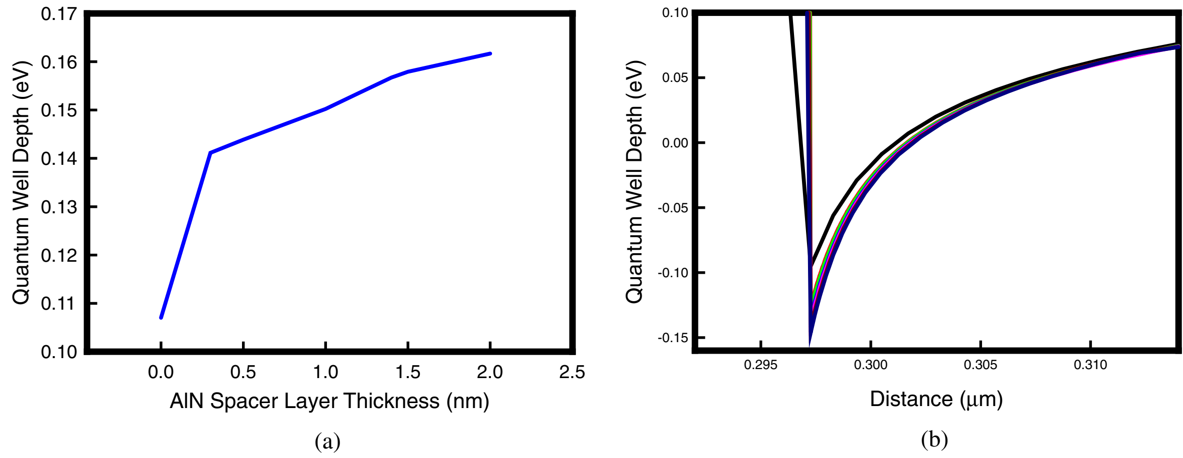

Fig. 5. (Color online) (a) Variation of the quantum well depth for the device at zero bias with respect to the different thickness of the AlN spacer layer. (b) Plot of the quantum well depth for the device at zero bias varying with the thickness of the AlN spacer layer.

Table IV. Simulated results of transport and DC characteristics for the device with respect to different thickness of AlN spacer layer.

AlN spacer layer thickness (nm)	2DEG depth (eV)	Electron concentration ($\times 10^{19}$ cm^{-3})	Mobility (cm^2 v^{-1} s^{-1})	Drain current (mA/mm)	Maximum transconductance (mS/mm)
0.0	0.095	0.89	1495	417	170
0.3	0.125	1.02	1673	451	180
0.5	0.128	1.11	1675	473	188
1.0	0.1346	1.31	1670	518	194
1.2	0.1378	1.37	1665	533	195
1.5	0.14213	1.45	1653	551	194
2.0	0.14614	1.58	1637	550	163

spacer layer. The results show that 2DEG's depth has 50% increases when the AlN spacr layer is 1.5 nm thick in the AlGaN/AlN/GaN HEMT.

2DEG, created at the hetero-interface on growing high band gap material $Al_{0.3}Ga_{0.7}N$ on comparatively small band gap material GaN, is crucial mechanism to confine electrons in quantum well which leads to high electron concentration and high mobility. It is found that large polarization fields in the AlN barrier layer in the AlN/GaN heterostructure results in high values of the 2DEG sheet density. The 2DEG's concentration in the AlGaN/AlN/GaN structure is given by[10)]

$$N_{2D} = \frac{\sigma_{AlN} + \left(\frac{\varepsilon_{AlN}}{\varepsilon_{AlGaN}}\right)\left(\frac{d_{AlGaN}}{d_{AlN}}\right)\sigma_{AlGaN} - \frac{1}{e}\left(\frac{\varepsilon_{AlN}}{d_{AlN}}\right)[E_f + \varphi_s + \Delta E_{c(AlGaN/AlN)} - \Delta E_{c(AlN/GaN)}]}{1 + \left(\frac{\varepsilon_{AlN}}{\varepsilon_{AlGaN}}\right)\left(\frac{d_{AlGaN}}{d_{AlN}}\right)}, \quad (11)$$

where σ_{AlGaN} is the polarization charge at AlGaN surface, φ_s is the depth of the Fermi level at the AlGaN surface with respect to its conduction band edge; ε_{AlGaN} and d_{AlGaN} are the dielectric constant and the thickness of AlGaN, respectively. High level of 2DEG's concentration is owing to the large conduction band offset and reduced wave propagation into the AlGaN layer[33)] caused by large band gap of the inserted AlN spacer layer. Device simulation results listed in Table IV and plotted in Fig. 6(a) show dependency of the conduction band offset on the thickness of AlN spacer layer improves the level of 2DEG's concentration. As shown in Fig. 6(a), the level of 2DEG's concentration increases with respect to the thickness of the AlN spacer layer. The level of 2DEG's concentration is improved by 63% when the thickness of the AlN spacer layer is 1.5 nm thick in the AlGaN/AlN/GaN interface. The electron concentration distribution for the device with respect to different thickness of the AlN spacer layer at $V_g = 0$ V, plotted in Fig. 6(b), shows the 2DEG distribution. Using the simulated data of electron density, the averaged position of 2DEG's distribution is further calculated by

$$\langle x \rangle = \frac{\int n \cdot x \, dx}{\int n \, dx}, \quad (12)$$

where n is the 2DEG's concentration and x is respective position.

Figure 7 shows the average position of 2DEG distribution. The results show that the averaged position of 2DEG's

© 2014 The Japan Society of Applied Physics

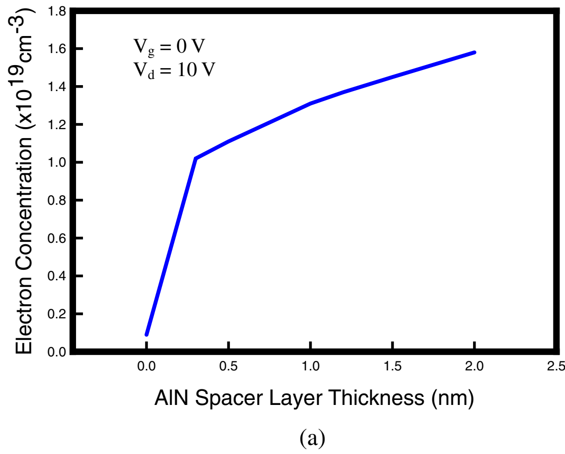

(a)

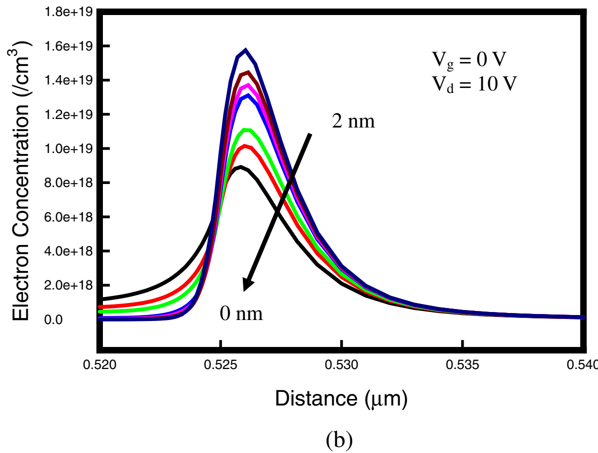

(b)

Fig. 6. (Color online) (a) Electron concentration for the device with different thickness of the AlN spacer layer at $V_g = 0$ V. (b) Electron concentration distribution for the device with respect to the thickness of the AlN spacer layer at $V_g = 0$ V.

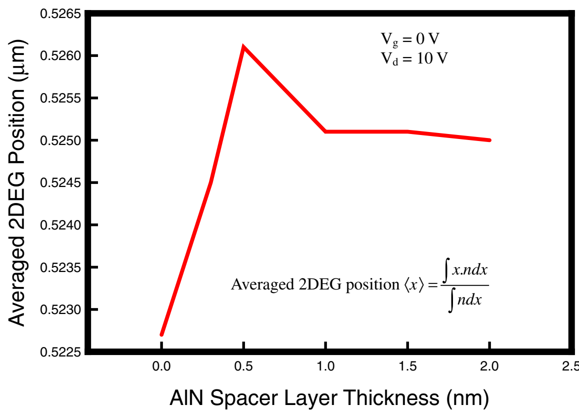

Fig. 7. (Color online) Averaged position of 2DEG's distribution calculated by using Eq. (11) with respect to the thickness of the AlN spacer layer.

concentration shift away from the interface on inserting AlN spacer layer, which indicates that the interface scattering is reduced. It has been known that the interface roughness is the main scattering mechanism when the level of 2DEG's concentration closes to the hetero-interface with the increase of the level of 2DEG's concentration.[34] As summarized in Table V, the average position of 2DEG's distribution shift

Table V. The position and shift of averaged 2DEG's distribution by using Eq. (11).

AlN spacer layer thickness (nm)	Averaged 2DEG position measured from surface (μm)	Shift of 2DEG (nm)
0.0	0.5227	
0.3	0.5245	1.8
0.5	0.5261	3.4
1.0	0.5251	2.4
1.2	0.5251	2.4
1.5	0.5251	2.4
2.0	0.5250	2.3

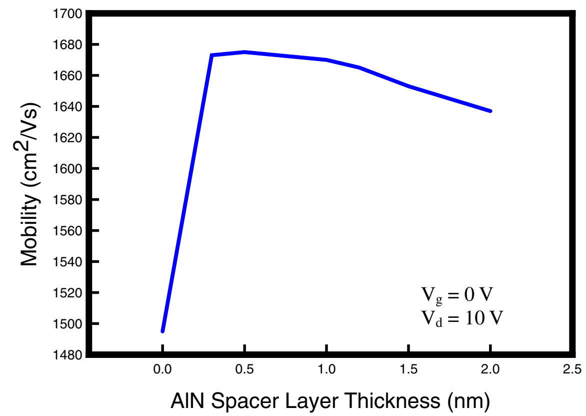

Fig. 8. (Color online) Plot of the variation of mobility versus the thickness of the AlN spacer layer.

away from interface attains on inserting thin AlN spacer layer in AlGaN/GaN interface which implies that the low interface roughness scattering on the AlGaN/AlN/GaN HEMTs in comparison with the conventional HEMTs. For the first time, the averaged position of 2DEG's distribution with respect to different thickness of the AlN spacer layer is calculated. Distance of averaged position of 2DEG's distribution attains its maximum when AlN thickness is 0.5 nm. Beyond this thickness, sufficiently high electron concentration leads the 2DEG position back toward the interface. Notably, the interface scattering reaches the minimum when the thickness of the AlN spacer layer is 0.5 nm thick and increase again on further increase the thickness. Therefore, mobility increase on increasing the AlN thickness, become maximum at the critical thickness and decrease beyond this thickness. The device simulation result depending on the electron mobility is affected by the thickness of the AlN spacer layer, as shown in Fig. 8. Simulation result shows that the 2DEG's mobility increases when the thickness increases from 0 to 0.5 nm. Our result shows that the mobility is increased by 12% when the 0.5-nm-thick AlN spacer layer is introduced in the AlGaN/GaN heterointerface. Low interface roughness and low alloy scattering mechanism increase the mobility. However, high carrier concentration at a thicker AlN spacer layer leads to moving 2DEG distribution toward the interface. It results in increase of the interface roughness scattering and coulomb scattering in 2DEG. Consequently, the mobility is decreased beyond 0.5-nm-thick AlN space layer.

© 2014 The Japan Society of Applied Physics

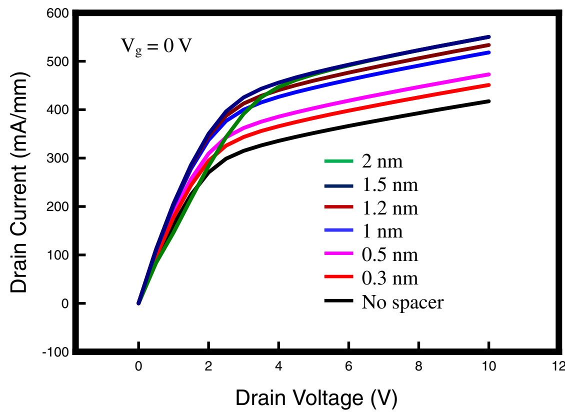

Fig. 9. (Color online) I_d–V_d curves for the device with respect to the different thickness of the AlN spacer layer (they are 0.0, 0.3, 0.5, 1.0, 1.2, 1.5, and 2.0 nm, respectively).

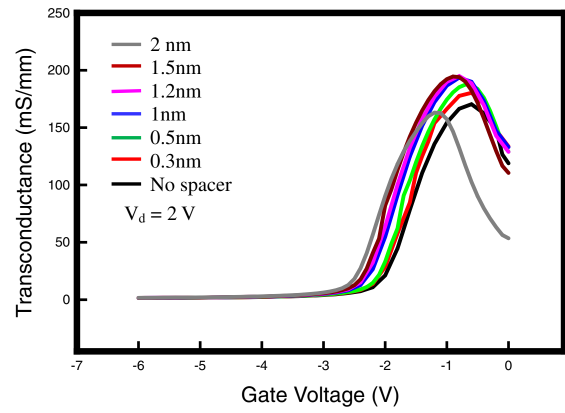

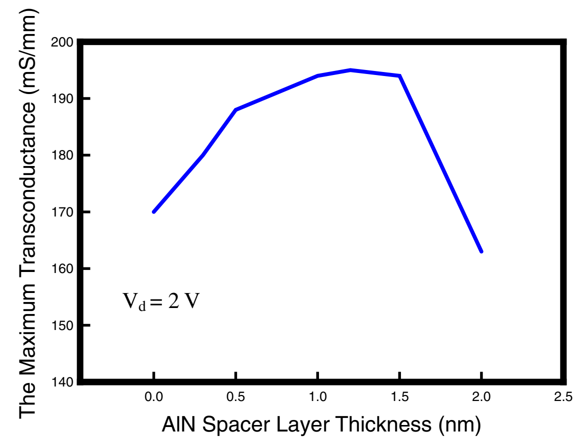

Fig. 10. (Color online) Plots of the (a) distribution of transconductance with respect to the gate voltage and (b) variation of transconductance with respect to the spacer layer thickness.

3.2 DC characteristics

Note that the AlGaN/AlN/GaN HEMTs show better DC characteristic in comparison with the conventional AlGaN/GaN devices[21,35] owing to excellent 2DEG property appearing in the AlGaN/AlN/GaN structures. Figure 9 shows that the simulated I_{ds}–V_{ds} curves for the AlGaN/AlN/GaN HEMT varing with the thickness of the AlN spacer layer at zero gate bias. We know that drain current is the result of the combined effect of mobility and electron concentration. Result shows that the drain current increases up to 0.5 nm spacer layer thickness due to increase of both electron concentration and mobility with spacer layer thickness. On increasing the spacer layer thickness from 0.5 to 1.5 nm, the drain current enhances due to the carrier concentration. Beyond the thickness of 1.5 nm, the drain current is lowered owing to decrease in the carrier's mobility. Our result shows that the drain current increases by 32% on using 1.5-nm-thick AlN spacer layer. Correspondingly, Fig. 10(a) shows the distribution of the transconductance with respect to the gate voltage. Figure 10(b) is the variation of the maximum transconductance with respect to the thickness of the AlN spacer layer. Figure 10(b) shows that the transconductance increases on the insertion of the AlN spacer layer in the AlGaN/GaN interface; it increases with the thickness is increased to 1.2 nm thickness of the AlN spacer layer. It slightly decreases from 1.2 to 1.5 nm thickness of the AlN spacer layer and rapidly decreases beyond this thickness. The maximal transconductance of 195 mS/mm is observed at the 1.2-nm-thick AlN space layer which is 15% increase, compared with the conventional the AlGaN/GaN HEMT. Beyond the 1.5-nm-thick AlN spacer layer, there is sizeable degradation of ohmic contact resistance because an AlN spacer layer with an extremely wide band gap decreases the contact resistance significantly.[20] The extremely high ohmic resistance in drain and source contacts degrade the device performance.

4. Conclusions

For the GaN HEMT with AlN spacer layer, the engineering findings of this study indicate that the 2DEG transport properties and DC characteristic of the AlGaN/AlN/GaN HEMTs are strongly affected by the thickness of the AlN spacer layer. The electron concentration significantly increases on the insertion of AlN spacer layer and is dependent on the thickness of the AlN spacer layer. The level of 2DEG's concentration is virtually moved away from the interface on inserting the AlN space layer. Distance between the 2DEG concentration and the interface attains its maximum at 0.5-nm-thick AlN space layer. This exhibits that the lowest interface scattering is observed at 0.5-nm-thick AlN space layer. The carrier mobility increases as the thickness of the AlN spacer layer and reaches its maximum at the thickness of 0.5 nm and decreases on further increase of thickness. Furthermore, drain current increases with the thickness is increased to 1.5 nm. Beyond this thickness, the drain current decreases owing to decrease in mobility. As the thickness of the AlN spacer layer is thicker than a critical thickness, the source and drain ohmic contacts are degraded and the drain current decreases. The maximum transconductance is observed at 1.2-nm-thick AlN spacer layer. High ohmic resistance makes lower transconductance beyond 1.5-nm-thick AlN space layer and finally degrades the device performance. Notably, 1.5-nm-thick AlN spacer layer can be used for high speed, high power switching device.

© 2014 The Japan Society of Applied Physics

Acknowledgements

This work was supported in part by the NCTU-UCB I-RiCE program, National Science Council (NSC), Taiwan under Contracts Nos. NSC 102-2221-E-009-161 and NSC 102-2911-I-009-302. Mr. N. M. Shrestha would like to thank Mr. T.-T. Luong for the sample grown.

1) L. Guo, X. Wang, C. Wang, H. Xiao, J. Ran, W. Luo, X. Wang, B. Wang, C. Fang, and G. Hu, Microelectron. J. **39**, 777 (2008).
2) A. Kranti, Rashmi, S. Haldar, and R. S. Gupta, Solid-State Electron. **46**, 1333 (2002).
3) E. T. Yu, G. J. Sullivan, P. M. Asbeck, C. D. Wang, D. Qiao, and S. S. Lau, Appl. Phys. Lett. **71**, 2794 (1997).
4) L. Hsu and W. Walukiewicz, J. Appl. Phys. **89**, 1783 (2001).
5) Y.-F. Wu, D. Kapolnek, J. P. Ibbetson, P. Parikh, B. P. Keller, and U. K. Mishra, IEEE Trans. Electron Devices **48**, 586 (2001).
6) Y.-F. Wu, B. P. Keller, P. Fini, S. Keller, T. J. Jenkins, L. T. Kehias, S. P. DenBaars, and U. K. Mishra, IEEE Electron Device Lett. **19**, 50 (1998).
7) J. Xie, J. H. Leach, X. Ni, M. Wu, R. Shimada, Ü. Özgür, and H. Morkoç, Appl. Phys. Lett. **91**, 262102 (2007).
8) M. Miyoshi, T. Egawa, H. Ishikawa, K.-I. Asai, T. Shibata, M. Tanaka, and O. Oda, J. Appl. Phys. **98**, 063713 (2005).
9) O. Ambacher, J. Smart, J. R. Shealy, N. G. Weimann, K. Chu, M. Murphy, W. J. Schaff, L. F. Eastman, R. Dimitrov, L. Wittmer, M. Stutzmann, W. Rieger, and J. Hilsenbeck, J. Appl. Phys. **85**, 3222 (1999).
10) T. R. Lenka and A. K. Panda, Indian J. Pure Appl. Phys. **49**, 416 (2011).
11) I. P. Smorchkova, C. R. Elsass, J. P. Ibbetson, R. Vetury, B. Heying, P. Fini, E. Haus, S. P. DenBaars, J. S. Speck, and U. K. Mishra, J. Appl. Phys. **86**, 4520 (1999).
12) R. Gaska, J. W. Yang, A. Osinsky, Q. Chen, M. Asif Khan, A. O. Orlov, G. L. Snider, and M. S. Shur, Appl. Phys. Lett. **72**, 707 (1998).
13) L. Wang, W. Hu, X. Chen, and W. Lu, J. Electron. Mater. **41**, 2130 (2012).
14) Y. Cao and D. Jena, Appl. Phys. Lett. **90**, 182112 (2007).
15) E. Bellotti, F. Bertazzi, and M. Goano, J. Appl. Phys. **101**, 123706 (2007).
16) D. C. Look, D. K. Lorance, J. R. Sizelove, C. E. Stutz, K. R. Evans, and D. W. Whitson, J. Appl. Phys. **71**, 260 (1992).
17) A. Teke, S. Gökden, R. Tülek, J. H. Leach, Q. Fan, J. Xie, Ü. Özgür, H. Morkoç, S. B. Lisesivdin, and E. Özbay, New J. Phys. **11**, 063031 (2009).
18) D. Jena, I. Smorchkova, A. C. Gossard, and U. K. Mishra, Phys. Status Solidi B **228**, 617 (2001).
19) I. P. Smorchkova, L. Chen, T. Mates, L. Shen, S. Heikman, B. Moran, S. Keller, S. P. DenBaars, J. S. Speck, and U. K. Mishra, J. Appl. Phys. **90**, 5196 (2001).
20) T. Nanjo, T. Motoya, A. Imai, Y. Suzuki, K. Shiozawa, M. Suita, T. Oishi, Y. Abe, E. Yagyu, K. Yoshiara, and Y. Tokuda, Jpn. J. Appl. Phys. **50**, 064101 (2011).
21) T. Ide, M. Shimizu, S. Hara, D.-H. Cho, K. Jeganathan, X.-Q. Shen, H. Okumura, and T. Nemoto, Jpn. J. Appl. Phys. **41**, 5563 (2002).
22) M. Miyoshi, A. Imanishi, T. Egawa, H. Ishikawa, K. Asai, T. Shibata, M. Tanaka, and O. Oda, Jpn. J. Appl. Phys. **44**, 6490 (2005).
23) T. Nanjo, M. Suita, T. Oishi, Y. Abe, E. Yagyu, K. Yoshiara, and Y. Tokuda, Appl. Phys. Express **2**, 031003 (2009).
24) J. D. Albrecht, R. P. Wang, P. P. Ruden, M. Farahmand, and K. F. Brennan, J. Appl. Phys. **83**, 4777 (1998).
25) R. Gupta and B. K. Ridley, Phys. Rev. B **48**, 11972 (1993).
26) R. Gupta, Turk. J. Phys. **23**, 551 (1999).
27) M. Farahmand, C. Garetto, E. Bellotti, K. F. Brennan, M. Goano, E. Ghillino, G. Ghione, J. D. Albrecht, and P. P. Ruden, IEEE Trans. Electron Devices **48**, 535 (2001).
28) K. C. Sahoo, C.-I. Kuo, Y. Li, and E. Y. Chang, IEEE Trans. Electron Devices **57**, 2594 (2010).
29) Y. Li, S. M. Sze, and T.-S. Chao, Eng. Comput. **18**, 124 (2002).
30) T.-W. Tang, X. Wang, and Y. Li, J. Comput. Electron. **1**, 389 (2002).
31) Y. Li and S.-M. Yu, Comput. Phys. Commun. **169**, 309 (2005).
32) S. Keller, S. Heikman, L. Shen, I. P. Smorchkova, S. P. DenBaars, and U. K. Mishra, Appl. Phys. Lett. **80**, 4387 (2002).
33) R. S. Balmer, K. P. Hilton, K. J. Nash, M. J. Uren, D. J. Wallis, D. Lee, A. Wells, M. Missous, and T. Martin, Semicond. Sci. Technol. **19**, L65 (2004).
34) J. Antoszewski, M. Gracey, J. M. Dell, L. Faraone, T. A. Fisher, G. Parish, Y.-F. Wu, and U. K. Mishra, J. Appl. Phys. **87**, 3900 (2000).
35) L. Yuan, W. Wang, K. B. Lee, H. Sun, S. L. Selvaraj, S. Todd, and G.-Q. Lo, World Acad. Sci., Eng. Technol. **69**, 127 (2012).

© 2014 The Japan Society of Applied Physics